Volume 11
Number 10
14 March 2023
Pages 2027–2278

Journal of Materials Chemistry B

Materials for biology and medicine

rsc.li/materials-b

ISSN 2050-750X

ROYAL SOCIETY OF CHEMISTRY

PAPER
Hong Liang, Rongsheng Tong, Yu Nie *et al.*
A cationic lipid with advanced membrane fusion performance for pDNA and mRNA delivery

10 YEARS ANNIVERSARY

Journal of Materials Chemistry B

ROYAL SOCIETY OF CHEMISTRY

PAPER

View Article Online
View Journal | View Issue

Cite this: J. Mater. Chem. B, 2023, 11, 2095

A cationic lipid with advanced membrane fusion performance for pDNA and mRNA delivery†

Yu Wei,‡[a] Ting He,‡[a] Qunjie Bi,[a] Huan Yang,[a] Xueyi Hu,[a] Rongrong Jin,[a] Hong Liang,*[bc] Yongqun Zhu,[d] Rongsheng Tong*[bc] and Yu Nie*[a]

Received 23rd December 2022,
Accepted 3rd February 2023

DOI: 10.1039/d2tb02783f

rsc.li/materials-b

The success of mRNA vaccines for COVID-19 prevention raised global awareness of the importance of nucleic acid drugs. The approved systems for nucleic acid delivery were mainly formulations of different lipids, yielding lipid nanoparticles (LNPs) with complex internal structures. Due to the multiple components, the relationship between the structure of each component and the overall biological activity of LNPs is hard to study. However, ionizable lipids have been extensively explored. In contrast to former studies on the optimization of hydrophilic parts in single-component self-assemblies, we report in this study on structural alterations of the hydrophobic segment. We synthesize a library of amphiphilic cationic lipids by varying the lengths (C = 8–18), numbers (N = 2, 4), and unsaturation degrees (Ω = 0, 1) of hydrophobic tails. Notably, all self-assemblies with nucleic acid have significant differences in particle size, stability in serum, membrane fusion, and fluidity. Moreover, the novel mRNA/pDNA formulations are characterized by overall low cytotoxicity, efficient compaction, protection, and release of nucleic acids. We find that the length of hydrophobic tails dominates the formation and stability of the assembly. And at a certain length, the unsaturated hydrophobic tails enhance the membrane fusion and fluidity of assemblies and thus significantly affect the transgene expression, followed by the number of hydrophobic tails.

Introduction

The great success of message RNA (mRNA) vaccines against the COVID-19 pandemic has highlighted the potential of nucleic acids (DNA or RNA) as therapeutics or vaccines in a wide range of diseases.[1] Gene therapies largely depend on whether the delivery carriers can efficiently deliver nucleic acid to the host cells *in vivo*. Considering the potential safety risks, production cost, and large-scale production, non-viral carriers have become the hot carriers in the marketization of gene carriers.

To date, lipid-based vehicles remain the first option to deliver genetic materials of interest. The mature technology and high biosafety promote its rapid product transformation.[2,3] For example, Onpattro® where small interfering (siRNA) is encapsulated in lipid nanoparticles (LNPs), was initially authorized by the U.S. Food and Drug Administration for polyneuropathy in 2018.[4] Recently, mRNA-LNPs based vaccines, Spikevax® (Moderna) and Comirnaty® (Pfizer/BioNTech) were approved for emergency prevention of COVID-19.[5] Typically, (ionizable) cationic lipids are the core components of LNPs, accounting for around 50% of the total lipids (molar ratio) and significantly affecting carriers' delivery performance.[6] However, these (ionizable) cationic lipids could form stable lipid carriers only in combination with helper lipids (phospholipids, PEGylated lipids) and/or cholesterol to achieve enough stability and membrane fusion properties.[7] With the multiple components in lipid carriers, it is challenging to evaluate the contribution of each lipid to the overall biological performance. In addition, it is labor-intensive, time-consuming, and less cost-effective to screen the optimal formulations.

The (ionizable) cationic lipids are generally amphiphilic, with an optimal balance between hydrophilic and hydrophobic segments. Notably, the hydrophilic head is important in gene transfection efficiency and cytotoxicity. Inspired by the cell-penetrating peptides (CPP) in viruses, several arginine-rich residues have been introduced into the hydrophilic segment of lipidic carriers. For instance, linear,[8] dendritic,[9] and clustered[10]

[a] National Engineering Research Center for Biomaterials/College of Biomedical Engineering, Sichuan University, Chengdu 610064, China. E-mail: nie_yu@scu.edu.cn
[b] Department of Pharmacy, Sichuan Academy of Medical Sciences & Sichuan Provincial People's Hospital, School of Medicine, University of Electronic Science and Technology of China, Chengdu 610072, China. E-mail: lianghong3689@163.com, 2207132448@qq.com; Fax: +86-28-8541-0246; Tel: +86-28-8541-2848
[c] Personalized Drug Therapy Key Laboratory of Sichuan Province, School of Medicine, University of Electronic Science and Technology of China, Chengdu 610072, China
[d] Life Sciences Institute and Innovation Center for Cell Signaling Network, Zhejiang University, Hangzhou 310058, China

† Electronic supplementary information (ESI) available. See DOI: https://doi.org/10.1039/d2tb02783f

‡ Equal contribution to the manuscript as co-first authors.

arginine all showed an enhanced transfection efficiency compared with controls. The guanidine of arginine could form bidentate hydrogen bonds with the negative phosphates, sulfates, and carboxylates on the cell surface and be driven into cells.[11] Our groups also did some explorations in screening the types and structures of amino acids and found that the structure, stability, size, and construction of assemblies also significantly affected the transfection efficiency of lipoplexes, especially in the presence of serum. As well, the hydrophobic tail of lipids mainly affects the assembly, which has been widely studied with a focus on the length (C), unsaturation (Ω), and the number of alkyl chains (N). However, their structure–activity relationship of these tails is still unclear or even in debate.

For example, Nakamura *et al.* found that cationic lipids containing longer unsaturated tails (C18:Ω1) induced a significantly improved silencing efficiency than their counterparts with shorter saturated ones (C14:Ω0 and C16:Ω0).[12] In contrast, J. Shi *et al.* reported that short saturated tails (C12:Ω0 and C14:Ω0) resulted in 2-fold higher pDNA transgene expression than longer unsaturated tails (C18:Ω1).[13] In addition, the architecture of the hydrophobic tail was found to be important. Some researchers reported that double-tailed cationic lipids showed about 10–20 fold higher gene transfection than single-tailed lipids in DNA delivery.[14] Interestingly, three-tailed lipids induced the most robust relative hit rate (%) than the double-tailed and four-tailed lipids in Cas9 mRNA delivery, because the large tails encouraged membrane fusion and phase transformation from lamellar phase to hexagonal (H_{II}) phase.[15] Although tremendous efforts have been placed to screen a relatively prominent material, a systemic and comprehensive comparison is also needed.

In this work, we synthesized a library of cationic lipids with the same cationic hydrophilic part and linker but varying hydrophobic part (alkyl chain length, number, and unsaturation degree). Such single-component cationic lipids were self-assembled into nanoparticles that were examined to deliver mRNA and plasmid DNA by studying their complexation ability, stability, conformation, cytotoxicity, as well as transgene efficiency both *in vivo* and *in vitro*.

Materials and methods

Experimental materials

Octanoic acid, lauric acid, palmitic acid, stearic acid, oleic acid, Boc-Arg(Pbf)-OH, triethylamine, di-*tert*-butyl decarbonate, and 2-(1*H*-Benzotriazole-1-yl)-1,1,3,3-tetramethyluronium tetrafluoroborate (TBTU) was obtained from LeYan (Shanghai, China). Methyl L-lysinate dihydrochloride and 2-(1*H*-benzotriazole-1-yl)-1,1,3,3-tetramethyluronium hexafluorophosphate (HBTU) were obtained from Adamas (Shanghai, China). Dimethyl sulfoxide (DMSO), dimethylformamide (DMF), dichloromethane (DCM), and methanol (MeOH) were bought from Greagent (Shanghai, China). Trifluoroacetic acid (TFA) was obtained from TCI (Shanghai, China). *N*-Ethyldiisopropylamine (DIEA) was bought from Astatech (Chengdu, China). 1,2-Dioleoyl-*sn-glycero*-3-phosphocholine (DOPC) was bought from Aladdin (Shanghai, China). 1,1′-Dioctadecyl-3,3,3′,3′-tetramethylindocarbocyanine perchlorate (DiI), 3,3′-dioctadecyloxacarbocyanine perchlorate (DiO), and cystamine dihydrochloride were obtained from Macklin (Shanghai, China). Branched polyethyleneimine (PEI, average M_w of 25 kDa) and 1,6-diphenylhexa-1,3,5-triene (DPH) were obtained from Sigma-Aldrich (Shanghai, China). Agarose was purchased from Biowest (Burgos, Spain). Dithiothreitol (DTT) was purchased from Beyotime (Shanghai, China). 50 × tris-acetate-EDTA buffer was obtained from Solarbio (Beijing, China). D-Luciferin potassium salt and PicoGreen dsDNA Quantitation Reagent were purchased from Yeasen (Shanghai, China). Quant-iT RiboGreen RNA Assay was obtained from Thermo (Waltham, America). Fetal bovine serum (FBS), minimum essential medium (MEM), and phosphate-buffered saline (PBS) were bought from Hyclone (Logan, America). Human cell lines, including hepatoma (HepG2), embryonic kidney (HEK293), and cervical carcinoma (HeLa), were purchased from the Chinese Academy of Science Cell Bank (Shanghai, China). Cell counter kit-8 (CCK-8) was obtained from Beyotime (Shanghai, China). Lipofectamine 2000 was obtained from Invitrogen (Carlsbad, America). Before use, all buffers were filtered (0.22 μm) in deionized water during preparation. The Endo-Free Plasmid Maxi Kit from Qiagen (Hilden, Germany) was used to purify the plasmid encoding enhanced green fluorescent protein (pEGFP). The luciferase gene in the pGL3 promoter was cloned into pcDNA3.1 to obtain plasmid pCMV-Luc. mRNA encoding enhanced green fluorescent protein (mEGFP) was obtained from the Yongqun Zhu group (Zhejiang University, China).

Chemical synthesis of a series of cationic lipids

Synthesis of the arginine-containing cationic segment. Boc-Arg(Pbf)-OH (5.5 g, 10.0 mmol), methyl L-lysinate dihydrochloride (1.3 g, 5.0 mmol), TBTU (4.4 g, 13.5 mmol), and DIEA (1.7 g, 13.5 mmol) were dissolved in DMF (30 mL). Then the reaction was reacted at 30 °C in an N_2 atmosphere overnight before the organic solution was removed in a vacuum. The residue was redissolved in DCM (250 mL) and washed twice with sodium chloride (NaCl) saturated solution. The organic phase was dried with magnesium sulfate ($MgSO_4$), and the solvents were removed using rotary evaporation in a vacuum. Compound **1** (5.0 g, 84% yield) was separated using a silica–gel chromatographic column (DCM/MeOH = 20/1, v/v) to yield a white powder.

Compound **1** (5.0 g, 4.2 mmol) was treated with a methanolic sodium hydroxide solution (0.8 g, 20.0 mmol) and stirred for 12 h. The organic phase was evaporated at low pressure, and dissolved in deionized water (10 mL), and the pH value was adjusted to 2–3 by diluted HCl (1.0 mol L^{-1}). Compound **2** was extracted by DCM and dried using anhydrous $MgSO_4$ (4.0 g, 79% yield).

Synthesis of the linker with disulfide bond. Triethylamine (1.8 g, 18.0 mmol) and cystamine (2.0 g, 9.0 mmol) were dissolved in MeOH (80 mL). Di-*tert*-butyl decarbonate (1.8 g, 8.0 mmol) was dissolved in MeOH (20 mL), slowly dropped into reaction mixture, and reacted overnight at 35 °C. After removing the organic solution, the residue was redissolved in

DCM (200 mL) and washed twice with NaCl saturated solution. The organic solution was dried with anhydrous $MgSO_4$, and the crude products were obtained by removing the solvent under low pressure. The crude products were separated by silica–gel chromatographic column (DCM/MeOH = 12/1, v/v) to get a white powder compound **3** (1.8 g, 79% yield).

Synthesis of different hydrophobic parts. Octanoic acid (4.1 g, 28.0 mmol), HBTU (12.2 g, 33.0 mmol), and DIEA (4.2 g, 33.0 mmol) were all dissolved in anhydrous DMF (40 mL). H-Lys-OMe·2HCl (3.0 g, 13.0 mmol) in anhydrous DMF (8 mL) was dropped into the reaction mixture and reacted at 30 °C under nitrogen for 12 h. After solution evaporation, the residuum was redissolved in DCM (250 mL). The solution was washed twice with NaCl saturated solution and dried with $MgSO_4$. The crude products were separated by a silica–gel chromatographic column (DCM/MeOH = 18/1, v/v) to get a white solid compound **4** (3.9 g, 75% yield).

Compound **4** (3.9 g, 9.5 mmol) was dissolved in MeOH (15 mL), followed by adding sodium hydroxide (1.0 mol L^{-1}, 10 mL) aqueous solution overnight at 30 °C. The residues were dissolved in water (5 mL) after the reaction solvent was evaporated, with the pH value adjusted to 2–3 by diluted HCl (1.0 mol L^{-1}). Compound **5** was extracted with DCM and dried with $MgSO_4$ (2.7 g, 72% yield).

Oleic acid was used to synthesize di-oleic acid with the same steps as compound **4** and compound **5**.

Compound **5** (2.7 g, 7.0 mmol), compound **3** (1.8 g, 7.0 mmol), DIEA (1.8 g, 14.0 mmol), and HBTU (5.2 g, 14.0 mmol) were dissolved in anhydrous DMF (50 mL) and reacted at 45 °C under nitrogen protection for 10 h. Under reduced pressure, the solvent was removed, and the solid was dissolved in DCM (200 mL). The solvent was dried with $MgSO_4$ after being washed with NaCl saturated solution. The crude products were separated using a silica–gel chromatographic column (DCM/MeOH = 15/1, v/v) to get a white solid compound **6** (3.2 g, 75% yield).

Compound **6** (3.2 g, 5.2 mmol) was dissolved in DCM (2 mL) and reacted continuously for 4 h at 30 °C with TFA (2 mL) added. After the solution was evaporated at low pressure, the obtained products were precipitated with ethyl ether and centrifuged at 8000 rpm for 3 min. After residual ethyl ether was removed in a vacuum, a yellow powder compound **7** (1.7 g, 60% yield) was obtained.

Synthesis of complete cationic lipids. Compound 2 (2.0 g, 1.6 mmol), DIEA (0.4 g, 3.4 mmol), and TBTU (1.0 g, 3.2 mmol) were dissolved in anhydrous DCM, then the compound **7** (0.9 g, 1.7 mmol) was added in anhydrous DMF. The reaction was carried out overnight at 30 °C under an N_2 atmosphere. The organic phase was removed and redissolved with DCM, then washed twice with saturated NaCl. The organic solvent was obtained and dried using anhydrous $MgSO_4$. The crude product was separated by a silica–gel chromatographic column (DCM/MeOH = 8/1, v/v) to obtain a white solid (1.7 g, 59% yield).

200.0 mg white solid was dissolved in anhydrous DCM (1.5 mL), then TFA (1.5 mL) was added dropwise and reacted for 12 h at 30 °C. The residues were precipitated with ice ether and collected by centrifugation after removing the solution in a vacuum. A white powder **RLS1** (85.0 mg, 74% yield) was obtained.

Lauric, stearic, palmitic, oleic, and di-oleic acid were substituted for octanoic acid to synthesize the other cationic lipids (**RLS2–6**).

RLS1 ^{1}H NMR (400 MHz, DMSO-d_6) δ (ppm) 4.09 (m, 2H), 3.38 (s, 2H), 2.97 (d, 4H), 2.74 (d, 4H), 2.12 (h, 2H), 2.02 (t, 3H), 1.79 (d, 5H), 1.41 (m, 13H), 1.23 (s, 20H), 0.85 (t, 6H). MS (MALDI-TOF), *m*/*z*: $[M + H^+]$ = 973.4525.

RLS2 ^{1}H NMR (400 MHz, DMSO-d_6) δ (ppm) 4.12 (s, 2H), 3.70 (s, 2H), 3.38 (s, 2H), 3.09 (d, 5H), 2.99 (s, 2H), 2.65 (m, 3H), 2.10 (t, 2H), 2.02 (t, 2H), 1.67 (s, 7H), 1.46 (s, 6H), 1.23 (s, 34H), 0.85 (t, 6H). MS (MALDI-TOF), *m*/*z*: $[M + H^+]$ = 1085.9045.

RLS3 ^{1}H NMR (400 MHz, DMSO-d_6) δ (ppm) 4.62 (m, 2H), 3.83 (q, 3H), 3.72 (t, 3H), 3.40 (d, 2H), 2.96 (m, 2H), 2.84 (d, 4H), 2.06 (m, 2H), 2.02 (t, 2H), 1.72–1.67 (m, 8H), 1.45 (m, 12H), 1.23 (s, 52H), 0.85 (t, 6H). MS (MALDI-TOF), *m*/*z*: $[M + H^+]$ = 1197.7869.

RLS4 ^{1}H NMR (400 MHz, DMSO-d_6) δ (ppm) 4.70 (d, 2H), 3.37 (m, 6H), 3.12 (s, 6H), 3.03 (s, 3H), 2.84 (d, 5H), 2.05 (d, 4H), 1.60 (s, 8H), 1.47 (s, 12H), 1.23 (s, 60H), 0.82 (m, 6H). MS (MALDI-TOF), *m*/*z*: $[M + TFA]^+$ = 1366.8543.

RLS5 ^{1}H NMR (400 MHz, DMSO-d_6) δ (ppm) 5.35 (m, 4H), 4.65 (m, 2H), 3.73 (s, 4H), 3.63 (m, 2H), 3.03 (s, 2H), 2.97 (m, 6H), 2.83 (d, 4H), 2.01 (m, 12H), 1.71 (s, 8H), 1.47 (s, 12H), 1.23 (s, 44H), 0.85 (t, 6H). MS (MALDI-TOF), *m*/*z*: $[M + H^+]$ = 1248.3542.

RLS6 ^{1}H NMR (400 MHz, DMSO-d_6) δ (ppm) 5.31 (t, 6H), 4.12 (s, 4H), 3.10 (s, 5H), 2.98 (s, 5H), 2.73 (s, 4H), 2.23 (m, 19H), 1.56 (m, 8H), 1.47 (d, 18H), 1.24 (s, 88H), 0.85 (t, 12H). MS (MALDI-TOF), *m*/*z*: $[M + H^+]$ = 2035.0947.

Preparation of gene complexes and related characterization

Assembly and characterization of cationic lipid assemblies. The injection approach was used to prepare cationic lipid assemblies.[16] Concisely, in 100 μL of DMSO, 1.0 mg of cationic lipid was dissolved and then added dropwise to deionized water (900 μL) with continuous and vigorous stirring for 1 h to form assemblies (1.0 mg mL^{-1}). The results of dynamic light scattering (DLS) were obtained by Zetasizer Nano ZS90 (Malvern Instruments, Worcestershire, England) to evaluate the particle size, zeta potential, and polymer dispersity index (PDI) of assemblies. The assembly morphologies were observed by transmission electron microscopy (TEM, JEM-2100Plus, JEOL, Japan).

Preparation and characterization of gene complexes

An equal volume of pDNA or mRNA (100 μg mL^{-1}) was added to the formed assemblies with various concentrations to obtain the desired N/P ratios, followed by a 20 minutes incubation period at room temperature before use. The physicochemical properties of lipid/pDNA lipoplexes were characterized by DLS.

Gene binding affinities

The gel retardation electrophoresis was used to assess the gene binding ability of lipid assemblies. Samples comprising 200 ng

pDNA were packed into 1% agarose gel, and electrophoresis was performed at an electric field of 85 volts for 40 minutes in 1 × tris–acetate–EDTA running buffer (20 mL 50 × tris–acetate–EDTA buffer with deionized water up to 1000 mL). The pDNA bands were observed with gel red staining and the Molecular Imager ChemiDoc XRS+ (Bio-Rad, America).

Lipoplexes containing pDNA and cationic lipid assemblies (1.0 mg mL^{-1}) (N/P 0-40) were incubated with 10 mmol L^{-1} DTT at 37 °C for 2 h. The release of cargo was then evaluated using gel electrophoresis under reducing environments.

Encapsulation efficiency

The mRNA encapsulation efficiency was calculated using the Quant-iT RiboGreen RNA Assay.[17] Firstly, the standard curve was drawn according to the reagent manual, using fluorescence intensity measurement by the BioTek Synergy H1 microplate reader (λ_{ex} = 480 nm, λ_{em} = 520 nm). The free mRNA was obtained by ultrafiltration centrifugation (5000 rpm) and followed with RiboGreen staining. Finally, the encapsulation efficiency was calculated as follows ("*W*" represented weight):

$$\text{Encapsulation}\% = \frac{W(\text{total mRNA}) - W(\text{free mRNA})}{W(\text{total mRNA})} \times 100\%$$

The encapsulation efficiency of pDNA was determined by PicoGreen reagent, which was similar to the mRNA encapsulation test.

Stability in serum

pDNA lipoplexes (N/P 20) were diluted to 1.0 mL with deionized water, with an ultimate pDNA concentration of 3.0 μg mL^{-1}. After incubation with 10% FBS for 0, 15, 30, 45, and 60 min, DLS was used to determine particle size. To examine the dissociation of pDNA, lipoplexes were incubated with 10% FBS, followed by gel electrophoresis.

Cell culture

HepG2, HeLa, and HEK293 cells were fostered in MEM medium included 10% FBS, 1% (v/v) penicillin/streptomycin (penicillin: 100 U mL^{-1}, streptomycin: 100 μg mL^{-1}), and 292 mg L^{-1} L-glutamine at 37 °C, 5% CO_2. Cells were detached from the bottom of the flask by incubating with trypsin-EDTA solution (0.25%/0.02%) when cell confluency was around 80–90%. For all *in vitro* studies, cell sowing density was 1 × 10^4 cells per well in 96-well plates before 24 hours until otherwise stated.

In vitro pDNA or mRNA lipoplexes transfection

Before transfection, fresh MEM medium with or without 10% FBS was transferred to each well to replace the original cell culture medium. Lipoplexes (10 μL per well, N/P 5–40) were applied to cells in each well (200 ng pEGFP per well). As controls, PEI/pDNA (N/P 10) and lipofectamine 2000/pDNA (0.5 μL/200 ng) were exposed to cells.

After 4 hours of incubation at 37 °C, the old medium was discarded, washed twice with PBS, and supplemented with MEM medium including 10% FBS. Cells were incubated for additional 44 hours. Positive EGFP cells were observed with an inverted fluorescence microscope (Olympus, Japan).

The transfection of mRNA in HeLa cells (200 ng per well) was similar to that of pDNA, and **RLS5** was used for intracellular transfection experiments with N/P ratios of 5–20. A fluorescence microscope and IVIS Lumina Series III imaging system were used to observe cells expressing EGFP.

In vitro cytotoxicity assay

In order to monitor the cytotoxicity of the cationic lipoplexes, the CCK-8 assay was used. Lipoplexes with various concentrations were exposed to cells for 24 hours at 37 °C, 5% CO_2. Then the serum-free medium was used to replace the original culture medium, and 10% CCK-8 was added for another 1 hour incubation. The results were measured by a microplate reader (Bio-Rad 550, USA) at 450 nm, and the cell viability was calculated using the following equation:

$$\text{Cellviability}(\%) = \frac{(A_s - A_b)}{(A_c - A_b)} \times 100\%$$

where A_s was the absorbance of the experimental cells exposed to lipoplexes, A_b was the absorbance of the non-treated cells, and A_c was the absorbance of the blank well without cells at 450 nm.

Membrane fusion experiments

8 nmol DiO dissolved in chloroform (100 μL) was mixed with 792 nmol cationic lipids in MeOH/chloroform (1/3, v/v, 1.0 mL), and dried by a rotary evaporator to formulate a thin film. PBS (pH 5.0) was added, vortexed for 5 min, and sonicated for 5 min to obtain DiO-labeled cationic lipid assemblies. The same method was used to obtain DiI-labeled DOPC vesicles.[18] Both DiI-labeled DOPC vesicles and DiO-labeled cationic lipid assemblies were incubated in 96-well plates, and the fluorescence emission spectra (480–600 nm) of the mixture were evaluated at various times using BioTek Synergy H1 microplate reader at an excitation wavelength of 440 nm.

100 μL DiI (5.0 μmol L^{-1}) was added to 1 × 10^4 HeLa cells and co-incubated for 20 min before washing off the excess dye with PBS to obtain the DiI-labeled HeLa cells. DiO-labeled cationic lipid assemblies were added to DiI-labeled HeLa cells and incubated for 30 min, and the membrane fusion phenomenon was observed by a confocal laser scanning microscope (TCS SP 5, Leica Co., Germany). The cells were detached with trypsin and transferred into a 96-well plate. The signal was observed under the förster resonance energy transfer (FRET) channel using a BioTek Synergy H1 microplate reader (λ_{ex} = 484 nm, λ_{em} = 565 nm).[18]

Membrane fluidity experiments

The membrane fluidity of six cationic assemblies was measured based on the fluorescence anisotropy of DPH (λ_{ex} = 360 nm, λ_{em} = 430 nm), which was incorporated in the lipid assemblies. The fluorescence spectrophotometer (FP-6500, JASCO Co., Tokyo, Japan) with a polarizing plate was used to detect the fluorescence signal. 10 μL DPH (100 μmol L^{-1}) in ethanol was added into lipid

assembly suspension (1.0 mL, 0.3 mmol L^{-1}). The following equation was used to calculate the polarity (P):

$$P = \frac{(I_{0°0°} - GI_{0°90°})}{(I_{0°0°} + GI_{0°90°})}$$

$$G = \frac{I_{90°0°}}{I_{90°90°}}$$

Membrane fluidity was expressed as $1/P$ because polarity was inversely proportional to fluidity.

Synchrotron-based small-angle X-ray scattering (SAXS)

SAXS experiments were executed at the Beijing Synchrotron Radiation Facility's (BSRF) beamline 1W2A (λ = 1.54 Å), with a Pilatus 1MF detector (169 mm × 179 mm). The detector was calibrated using a standard carbon fiber sample and a standard silver behenate sample. X-ray scattering intensity patterns were captured while the samples were exposed to the synchrotron beam for 20 s. The 2D scattering data were transformed into 1D profiles using the Fit2D program.[19]

In vivo transfection

pDNA transfection. Female BALB/c nude mice, 6-week-old, weighing 18–20 g, were purchased from GemPharmatech LLC. (Jiangsu, China). All animal experiments were approved by Ethics Committee for Biomedical Research and conducted in accordance with the Guidelines for Care and Use of Experimental Animals of West China Hospital. BALB/c mice were divided into groups and placed in a pathogen-free animal laboratory. Before the experiment, BALB/c mice were acclimatized to the new environment for 5 days. Mice were divided into 4 groups (n = 5) treated with saline, **RLS5**/pDNA, PEI/pDNA, and naked pDNA, respectively. 100 μL **RLS5**/pDNA (N/P 20) containing 20 μg pGL3 was intramuscularly injected into the hind leg of each mouse. As controls, 50 μL PEI/pDNA (N/P 10) and naked pDNA containing 20 μg pGL3 were also administrated. At defined time points (days 1, 2, 3, 5, and 7 post-administration), 150 μL D-luciferin potassium salt (15 mg mL^{-1}) was injected intraperitoneally into each mouse 10 min before imaging. An IVIS Lumina Series III imaging system was used to perform bioluminescence imaging. Molecular Imaging software quantified the intensity of bioluminescence signals emanating from pDNA expression at the injection site.

RNA transfection. BALB/c nude mice were divided into different groups (n = 5) and dosed with **RLS5**/mRNA lipoplexes (N/P 10, 100 μL) containing 20 μg mEGFP, naked mEGFP (20 μg) and saline alone through intramuscular injection into the hind legs of each mouse. At defined time points (days 1, 2, 3, 5, and 7 post-administration), fluorescent luminescence imaging of mEGFP using an IVIS Lumina Series III imaging system (λ_{ex} = 450 nm, λ_{em} = 509 nm). The quantification of fluorescent signal intensity was performed the same as pDNA transfection.

Results and discussion

Synthesis of six cationic lipids

According to our previous work, cationic lipids with dendritic arginine promoted cellular membrane penetration, and the linker of disulfide bonds induced a rapid release of pDNA under intracellular reduction conditions.[9,20] Given that the hydrophobic portion of cationic lipids plays key roles in particle assembly, size, fluidity, as well as *in vivo* transfection,[21,22] we synthesized six cationic lipids with different hydrophobic parts but sharing the same dendritic arginine-rich head and disulfide linker (Fig. 1). In detail, the hydrophobic parts differ in (1) lengths of the alkyl chain (numbers of carbon atoms, C = 8–18), (2) numbers of alkyl chains (dual or quadruple tails, N = 2, 4), and (3) degrees of unsaturation (Ω = 0, 1). MALDI-TOF-MS and ^{1}H NMR were used to identify the molecular structure (Fig. S13–S18, ESI†).

Characterization of lipid assemblies

First, lipid assemblies were characterized by DLS in terms of hydrodynamic diameters and ζ potential. As Fig. 2(A) displayed, all six cationic lipid assemblies were 140–220 nm in hydrodynamic diameter. For the lipid assemblies with the same saturated (Ω0) dual alkyl chains (**RLS1–4**), their Z-average particle sizes increased with prolonged alkyl chain length,[13] ranging from 140 nm (C8), 164 nm (C12), 187 nm (C16), to 212 nm (C18) (Fig. 2(A) and Table S1, ESI†). In contrast, the particle size decreased with an increased unsaturation degree of cationic lipids comprising the same alkyl chain length and number (**RLS4**, C18:Ω0:N2 *vs.* **RLS5**, C18:Ω1:N2). This might be due to the folding effect of alkyl chains caused by the unsaturated bonds.[23] In a direct comparison between **RLS5** and **RLS6** (C18:Ω1:N4) with the same alkyl chain length and unsaturation, lipids with 4 alkyl chains assembled into larger particles than their counterpart containing 2 alkyl chains. The TEM images (Fig. S5, ESI†) showed that the assemblies could form spherical shapes. The particle size measured by TEM was smaller than the results of DLS, which might be attributed to the fact that the particle size measured by DLS was obtained in the state of hydration.[24]

The hydrophilic head mainly determined the ζ potential of cationic lipid assemblies. Thus, the ζ potentials of the six cationic lipid assemblies were all positive, between +21–27 mV (Fig. 2(A)).

Then, we investigated the particle size and ζ potential of pDNA complexes at various N/P ratios from 10 to 40 (Fig. 2(B) and (C)). The particle size of the lipoplexes decreased slightly as the N/P ratio increased. At a higher N/P ratio, pDNA could be more firmly compacted into particles with smaller sizes, which was consistent with the literature.[25] In addition, almost all cationic lipid assemblies could compress pDNA below 300 nm at various N/P ratios, except for **RLS1**/pDNA (N/P 10, 576 nm). The results indicated that relatively high surface ζ potential required fewer assemblies for pDNA compression.

Next, the gel retardation method was used to test the compression capacity of the cationic lipid assemblies (Fig. 2(D)).

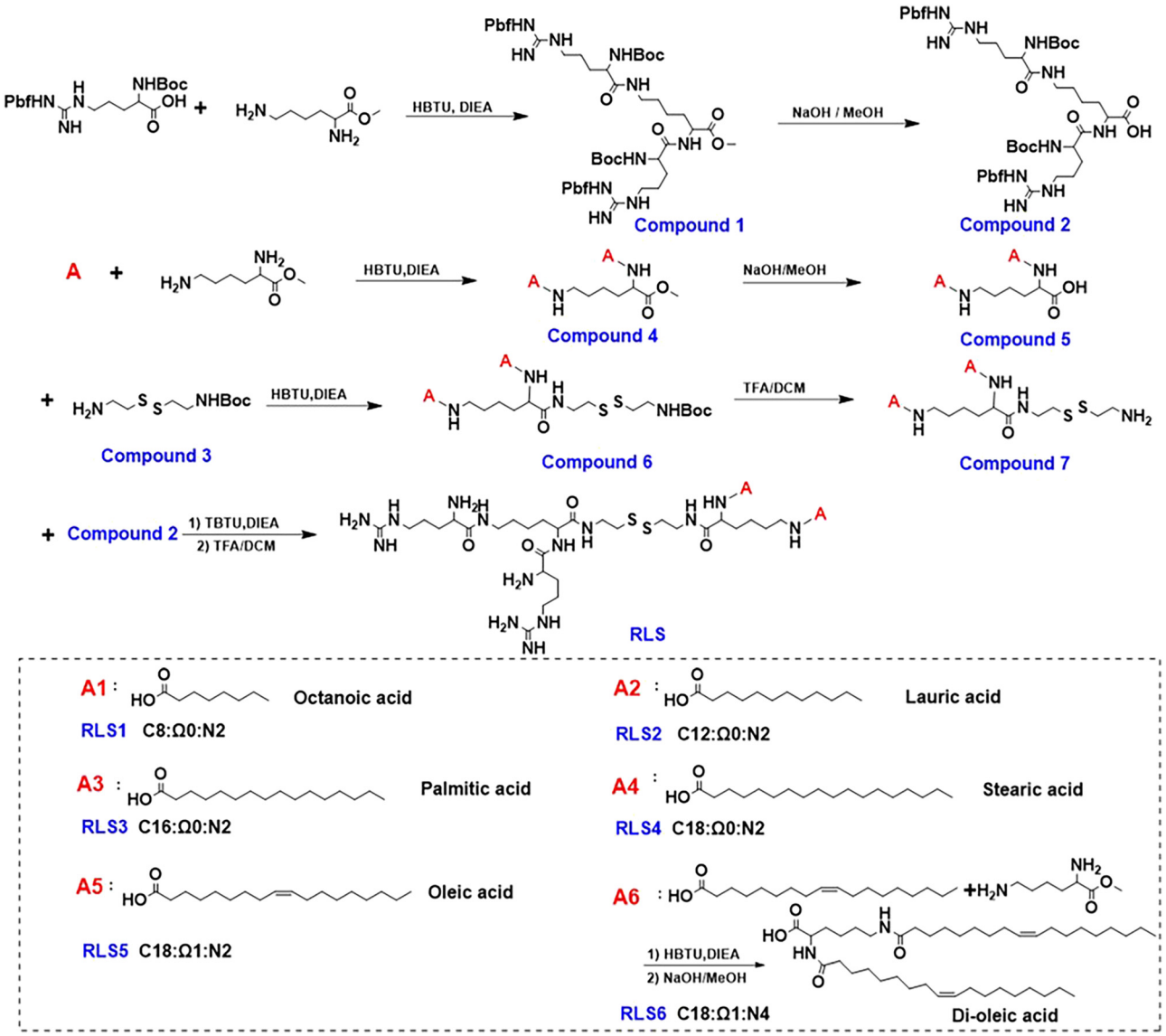

Fig. 1 Synthesis of a series of cationic lipids with the same dendritic arginine peripheries and varied hydrophobic segments. *C*: length of alkyl chains; *Ω*: unsaturation of alkyl chains; *N*: number of alkyl chains.

We found that **RLS1** with the shortest hydrophobic parts (C8) only fully compressed pDNA at a higher N/P ratio (20), compared to other lipids (**RLS2–6**) with longer hydrophobic parts that a full complexation was found at N/P 5. This might be due to the fact that the short hydrophobic length (C8) could not form a stable lipid assembly in the process of hydration.[26] PicoGreen and RiboGreen reagents were used to assess the encapsulation efficiency of pDNA and mRNA, respectively. The results showed that the encapsulation efficiency of **RLS1–6**/pDNA (N/P 20) were 95.43%, 96.15%, 95.18%, 97.05%, 96.39%, and 98.44%, respectively. And the encapsulation efficiency of **RLS5**/mRNA (N/P 5) was 96.03% (Fig. S6 and Table S2, ESI†).

In order to achieve efficient gene delivery, sufficient intracellular release was of significance.[27,28] We thus investigated pDNA release from lipoplexes in the presence of 10 mmol L^{-1} DTT by a retardation electrophoresis assay using agarose gel (Fig. S7, ESI†).[29] The results demonstrated that pDNA was isolated from cationic lipids in an intracellular reduction environment, and free/naked pDNA bands could be observed after incubation for 2 hours. As previously reported, we believed that the disulfide bond breakage provided a prerequisite for releasing genes in carriers.[20]

Stability in serum

Under physiological conditions, the interaction between serum proteins and lipids affected the stability of lipoplexes. Negatively charged biomacromolecules (*e.g.*, albumin) potentially bind onto the cationic lipoplexes, leading to aggregation, precipitation, or disintegration of the lipoplexes consequently resulting in transfection failure. Thus, serum resistance was essential for cationic lipoplexes.[30] After incubation with serum, we evaluated the stability of pDNA lipoplexes (**RLS1–6**) in size

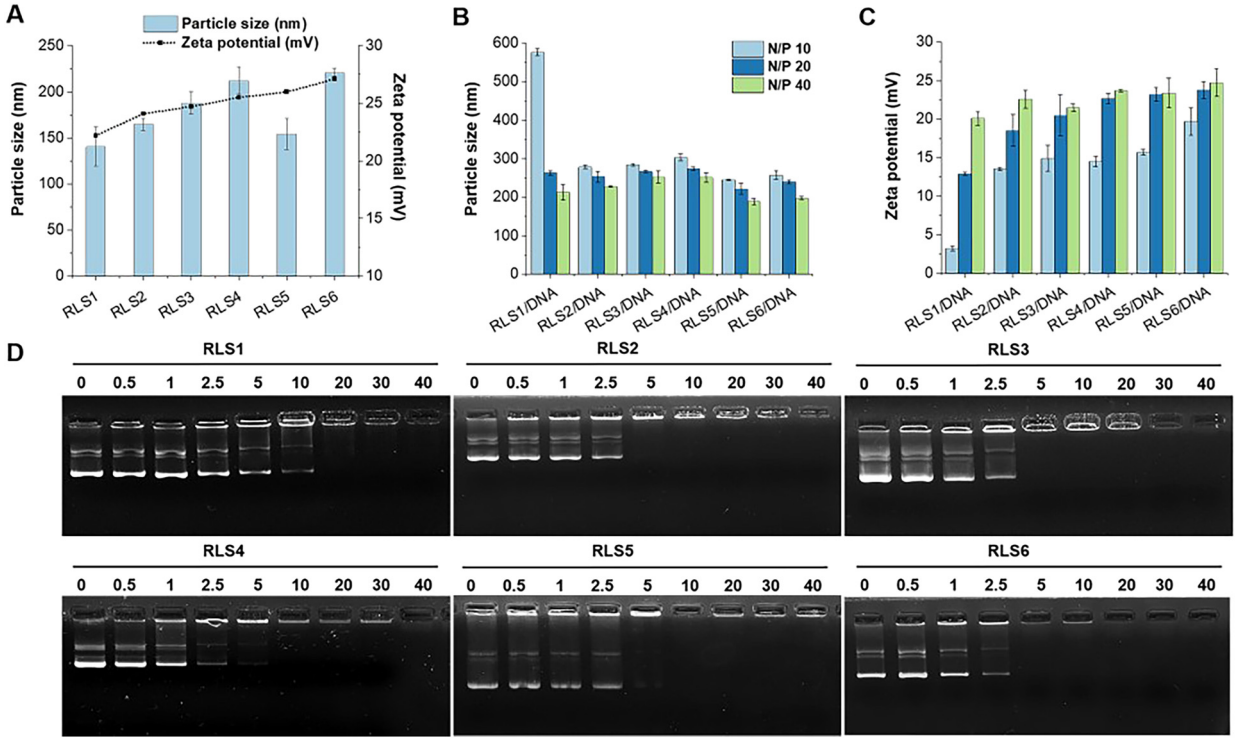

Fig. 2 Particle size, zeta potential, and gene compression. (A) Particle size and zeta potentials of lipid assemblies. Particle size (B) and zeta potential (C) of lipid gene complexes at various N/P ratios. Data represent mean ± SD (n = 3). (D) Gel electrophoresis assay of cationic assemblies/pDNA complexes at different N/P ratios.

and pDNA release (Fig. 3 and Fig. S8, ESI†). Obviously, lipoplexes based on **RLS1**, **2**, and **3** aggregated after exposure to FBS, whereas other lipoplexes did not significantly differ along with incubation time. At the beginning (0 min), the particle size of all cationic lipoplexes was between 200–250 nm. With the increase of time, the size of **RLS1–3** fluctuated obviously, and the fluctuation range decreased with the increase in the length of alkyl chains. After continuous incubation, the size of **RLS1** reached almost 1 μm with poor dispersion (PDI = 0.72), and the maximum size of **RLS2** and **RLS3** was also up to about 500 nm (PDI = 0.45) and 400 nm (PDI = 0.48), respectively (Table S3, ESI†). In contrast, the particle size of **RLS4–6** remained unchanged, representing good stability in serum. Gel electrophoresis assays (Fig. S8, ESI†) showed that partial pDNA was released from **RLS1–3** lipoplexes, which might be the reason for the serious particle size variation. Gilmore *et al.* found that the serum stability of lipids was related to the force required to stretch the lipids laterally.[31] We speculated that **RLS4–6** showed good serum stability due to its long carbon chain and increased intermolecular van der Waals force, resulting in high stability of the whole lipid molecule and no deformation.[32]

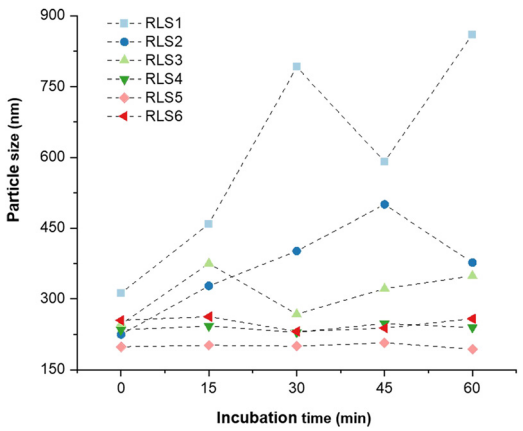

Fig. 3 The particle size of lipid gene complexes after 0, 15, 30, 45, and 60 min of incubation with 10% FBS.

Cytotoxicity of six cationic lipoplexes

The cytotoxicity of those cationic lipoplexes was assessed by CCK-8 assay. We found that over 90% of cells survived after exposure to all those six lipoplexes, regardless of cell lines (Fig. S9, ESI†). In general, six cationic lipids have satisfying cell survival viability, which might attribute to the introduction of disulfide bonds in the carrier. Our previous work has shown that the cytotoxicity of cationic lipid assemblies without disulfide bonds was much higher than that of cationic lipid assemblies containing disulfide bonds.[20] The cytotoxicity of cationic lipids was mainly from the poor metabolism or decomposition of gene carriers by cellular enzymes. Gene carriers with disulfide bonds could be broken into fragments and easily excreted from the body without significant toxicity.[33]

Transfection efficiency *in vitro*

Transfection efficiency of pEGFP *in vitro* was assessed on HEK293, HepG2, and HeLa cells at various N/P ratios with or

without 10% FBS. Lipofectamine 2000 and PEI were used as controls (Fig. 4 and Fig. S10–S12, ESI†). The transfection efficiency of **RLS1–3** was very low, and the gene expression of **RLS4** with the longest saturated alkyl chains showed a slight increase (Fig. 4(A)). This trend was consistent in HEK293 and HepG2 cells (Fig. S10 and S11, ESI†). **RLS5** and **RLS6** showed far superior to **RLS1–4** and the control groups in both HEK293 and HepG2 cells. The difference between **RLS5** and **RLS6** was displayed in HeLa cells (Fig. S12, ESI†). In the presence of FBS, **RLS5** had significant transfection performance advantages over **RLS6**, whereas, without FBS, they achieved similar transfection efficiency. This indicated that an increased number of tails slightly decreased transfection efficiency. In short, the lipoplexes based on cationic lipids **RLS5** and **RLS6** with unsaturated alkyl chains had prominent transfection efficiency in different cells.

Quantitative analysis by Imaging J software also confirmed the superiority of **RLS5** and **RLS6** in transfection, showing up to 7-fold and a 3.8-fold increase compared with that of **RLS1–4** in the presence (Fig. 4(B) and (C)) and absence (Fig. 4(E) and (F)) of FBS. On HeLa cells, **RLS5** resulted in 1.5-fold (with FBS) and 4-fold (without FBS) higher gene expression than that of **RLS6** (Fig. 4(D) and (G)). Thus, we further evaluated the delivery efficiency of mRNA on HeLa cells. Excitingly, **RLS5** showed superior green fluorescence protein expression at a very low N/P ratio (5) in the presence of FBS (Fig. 5(A) and (B)), which was 5-fold higher than lipofectamine 2000 (Fig. 5(C)).

While the transfection effect of four cationic lipids (**RLS1–4**) with the saturated hydrophobic part in different cells was not good, **RLS4** (C18) with the longest carbon chain had relatively better transfection efficiency, which seemed to be related to its stability. In addition, we found that the unsaturation of the hydrophobic part of cationic lipids significantly affected the transfection efficiency, followed by the number of hydrophobic tails. The unsaturated structures disrupted the regular packing of the cellular membrane and facilitated the escape of nucleic acid within the cell.[34,35] Meanwhile, an excessive number of hydrophobic parts might lead to more hydrophobicity and thus prevent the carriers from entering the cell surface.[36]

Much work has been carried out to optimize the hydrophobic part of lipids but without solid conclusions.[24,37] Most studies found that cationic lipids with shorter saturated alkyl chains or unsaturated alkyl chains[38] were crucial for acquiring splendid transfection efficiency since they were in charge of membrane fluidity. However, a degree of rigidity for the membrane was also needed to stabilize the lipid assemblies,[39] and long-chain lipids would likely strengthen the stability.[22] We assumed that the striking transfection effect of **RLS5** was due to its long-chain stability and the introduction of unsaturated bonds that allowed it to have good fluidity. In order to explore the underlying mechanism leading to this result, we have carried out an in-depth exploration at the molecular level.

Study on the molecular mechanism

Gene delivery must overcome several biological barriers to achieve efficient transfection, including cellular attachment, plasma membrane penetration, endosomal degradation prevention, *etc.* The cellular entry mechanism of lipid carriers was still controversial. Some studies reported endocytic pathway was the primary means,[40] and others suggested cellular membrane fusion was dominant.[41] In addition, the pathway of endosomal escape (a critical step in gene release into the cytoplasm) of lipid gene carriers also has different interpretations. Nevertheless, the interaction of lipid carriers with biological membranes (cellular and endosomal membranes) was crucial for gene delivery, especially the stability and fluidity of lipid carriers. Therefore, we explored

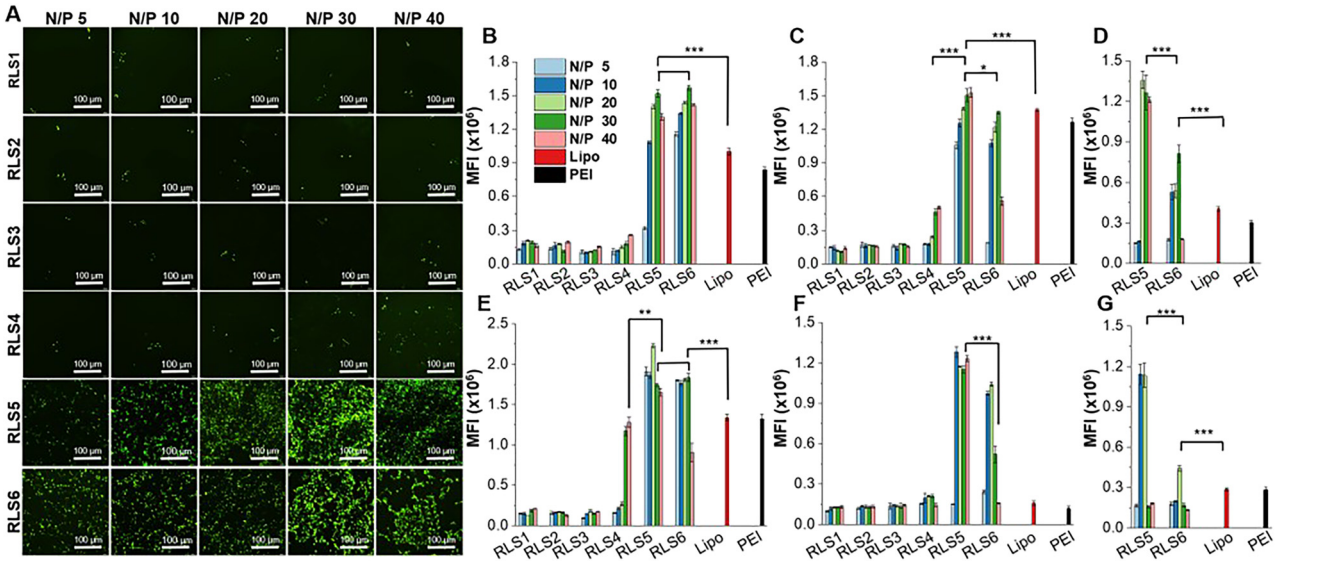

Fig. 4 Transfection efficiency of pEGFP on various cells (HEK293, HepG2 and HeLa). (A) Fluorescence microscopy images of cells with pEGFP transfection on HEK293 cells with 10% FBS, scale bar was 100 μm. Quantitative transfection efficiency in different cells: HEK293 with 10% FBS (B) and without FBS (E), HepG2 with 10% FBS (C) and without FBS (F), HeLa with 10% FBS (D) and without FBS (G). (*$p < 0.05$, **$p < 0.01$, ***$p < 0.001$)

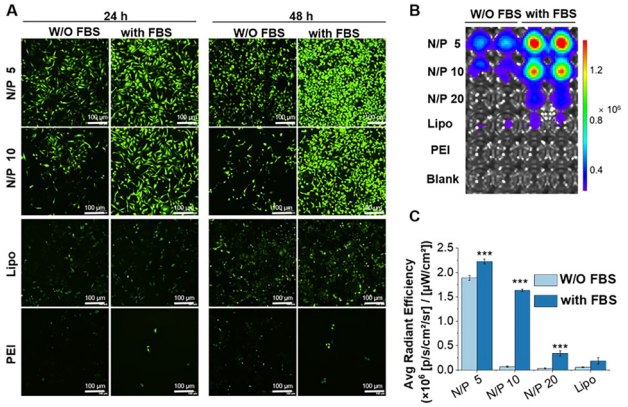

Fig. 5 The transfection effect of mEGFP delivered by **RLS5** in HeLa cells. The fluorescence images were observed by fluorescence microscope (A) and fluorescence imaging using IVIS Lumina Series III imaging system (B). (C) Quantitative transfection efficiency in HeLa cells. The scale bar was 100 μm. (***$p < 0.001$ *vs.* lipo with 10% FBS, W/O: without).

the membrane fusion, fluidity, and crystal conformation of six lipids for their stability and fluidity.

Membrane fusion

The whole transfection process depends on "membrane interactions", in which the membrane of the lipoplexes first interacts with the plasma membrane for internalization and then with the endosomal membrane to trigger the release of the nucleic acid cargo. Thus, we first investigated plasma membrane fusion using the FRET strategy with donor and acceptor fluorescent labeling. Gene complexes labeled with DiO as the donor was incubated with HeLa cells labeled with DiI as the acceptor to form FRET pairs (Fig. 6(A)). During the incubation, we could hardly detect red fluorescence in **RLS1–3** groups under the FRET channel of the confocal laser scanning microscope (Fig. 6(B)). Because the distance between the two fluorescent labels was not close enough to produce the FRET phenomenon, indicating no plasma membrane fusion. Whereas cells incubated with **RLS4–6** exhibited strong red fluorescence under FRET channels, resulting from the occurrence of membrane fusion. Quantitative data was showed in Fig. 6(C).

After endocytosis, the internalized substances were usually trapped in vesicles and eventually degraded within the endosomal compartments. Efficient endosomal escape was important

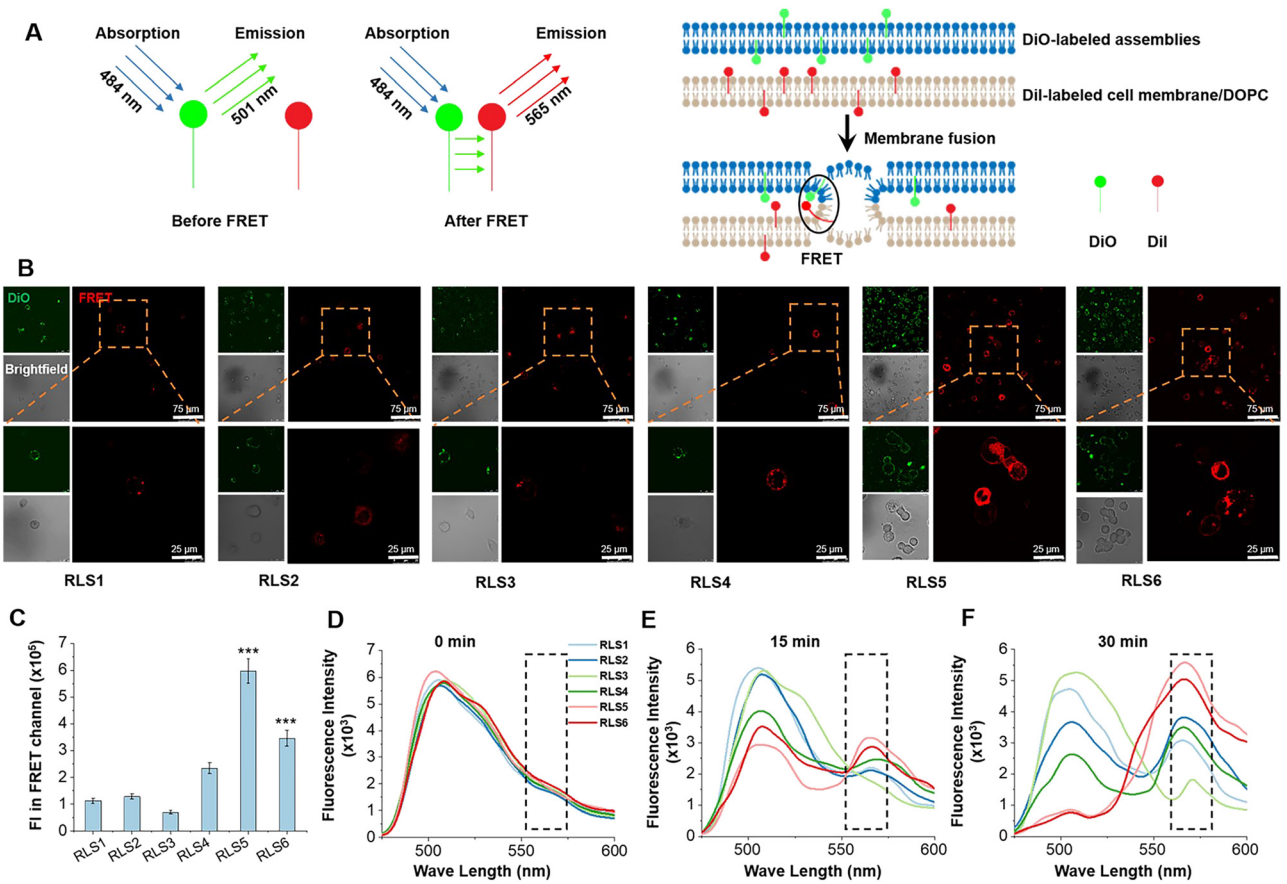

Fig. 6 Membrane fusion effect of six cationic lipid assemblies in HeLa cells and simulated endosomal membrane. (A) Mechanism of FRET in membrane fusion. (B) The FRET effect in HeLa cells was observed by confocal laser scanning microscope after incubation for 30 min. Assemblies were labeled with DiO and cell membranes were labeled with DiI. The orange box indicated partial magnification. (C) FRET evaluation by measuring fluorescence intensity (FI). Data were the mean ± SD ($n = 3$, ***$p < 0.001$ *vs.* **RLS4**). (D)–(F) FRET emission peak (565 nm) under simulated conditions between DiO-labeled assemblies and DiI-labeled DOPC vesicles with different incubation times (0, 15, and 30 min).

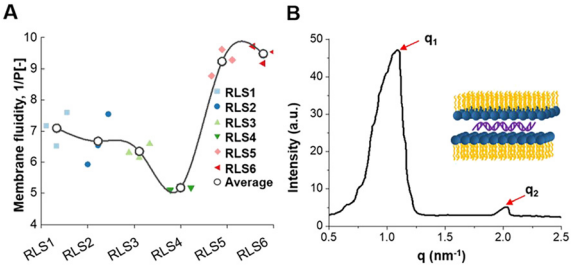

Fig. 7 Molecular mechanism exploration on cationic lipid assemblies. (A) Membrane fluidity ($1/P$ [–]) of six lipid assemblies was performed by fluorescence spectrophotometer at room temperature 25 °C. (B) Small-angle X-ray scattering profiles of **RLS5** at room temperature. The peak position ratio of q_1 and q_2 was 1 : 2, which indicated the formation of well-ordered lamellar structures.

for gene transfection. We further mimicked the endosomal/lysosomal membrane fusion using DiI-labeled DOPC vesicles in acidic conditions (pH 5.0). In **RLS1–4**, the fluorescence intensity of the donor at 501 nm did not decrease significantly, and the intensity of the acceptor at 565 nm did not increase significantly. It suggested that the fusion effect of these four cationic lipids was incomplete and slow. Whereas **RLS5** and **RLS6** showed a rapid increase in fluorescence intensity at the emission wavelength of 565 nm, indicating an excellent fusion with the simulated endosomal membrane (Fig. 6(D)–(F)). So, the transfection results were consistent with the fusion effect, which also confirmed that the satisfying transfection efficiency of **RLS5** and **RLS6** was mainly due to their complete and rapid membrane fusion with the endosomal membrane after the cytoplasm successfully.

Membrane fluidity

Membrane fluidity affected the fusion of endosomal membranes, which was necessary for the endosome escape of genes.[42] As **RLS5-6** showed the best membrane fusion ability, we further explored their fluidity. Membrane fluidity for various lipid assemblies was evaluated using a fluorescence probe DPH.[43] The $1/P$ was the reciprocal polarization obtained by DPH fluorescence analysis, which reflected the fluidity of the membrane. Our experimental results showed that among the six lipids, only **RLS5** ($1/P = 9.2$) and **RLS6** ($1/P = 9.6$) had higher fluidity (Fig. 7(A)). It was probably due to the existence of unsaturated bonds increased fluidity by preventing the tight accumulation of lipids.[44] In addition, a gradual decrease in fluidity could be seen with increasing alkyl chain length among the four cationic lipids containing saturated alkyl chains because short-chain lipids tended to separate in the bimolecular clusters or "rafts" form in the layer, resulting in an uneven distribution of lipids across the membrane. Although the fluidity of **RLS1–4** was slightly different, these $1/P$ values were generally around 6. From the fluidity results, the length and number of alkyl chains in the hydrophobic part had no significant effects on lipid fluidity. However, increasing the unsaturation improved the overall fluidity of the lipids and thus significantly improved their gene transfection effects.

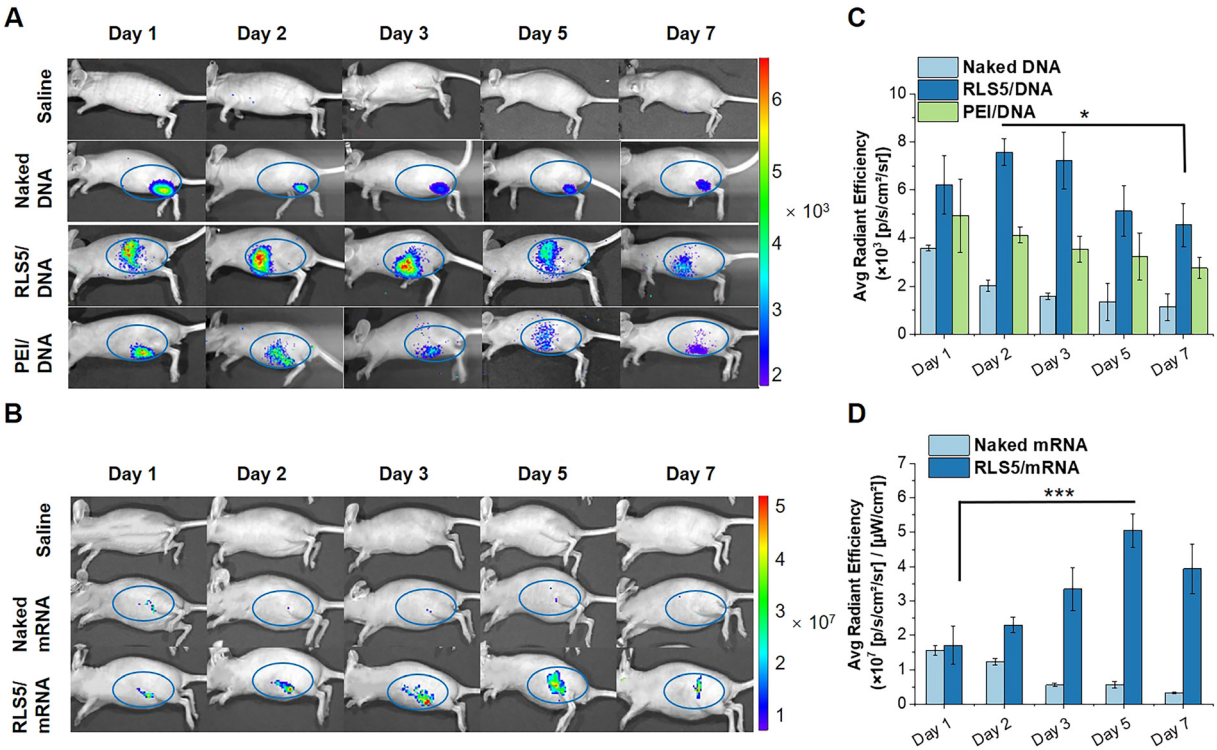

Fig. 8 Transfection efficiency of pGL3 and mRNA *in vivo* after intramuscular injection. pGL3 (A) and mEGFP (B) *in vivo* expression efficiency at different time points after intramuscular injection by fluorescence imaging using IVIS Lumina Series III imaging system (the blue circle indicated the injection site). Quantitative fluorescence intensity in the blue circle of pGL3 (C) and mEGFP (D) expression *in vivo*. (*$P < 0.05$, ***$P < 0.001$).

Crystal phase

In addition to the membrane fusion and fluidity discussed above, crystal conformation was an essential factor that should not be ignored. According to reports, the lamellar phase benefited the stability of lipid carriers, while the hexagonal (H_{II}) phase benefited the fusion with biological membranes.[45] Therefore, we utilized the SAXS technique to investigate the crystal phase of **RLS5**. The X-ray scattering patterns of **RLS5** showed a peak ratio of 1 : 2 (Fig. 7(B)), which was characteristic of the lamellar phase. This lamellar phase probably made the delivery system less susceptible to dissociation in complicated biological environments, facilitating stability in serum and efficient gene transfection *in vivo*.

Through the above experiments, **RLS5**, with a stable lamellar phase, showed the best lipid membrane fusion and overall fluidity, which might be the reason for the outstanding *in vitro* transfection efficiency in serum.

Animal experiments

Further, we investigated the transfection effects *in vivo*. pCMV-Luc encoding luciferase was complexed into lipoplexes and intramuscularly injected into BALB/c nude mice. At day 1, 2, 3, 5, and 7 after administration, transgene expression was determined by intraperitoneal injection of D-luciferin potassium salt. As shown in Fig. 8(A) and (C), a notably higher bioluminescent signal was found in the mice injected with **RLS5**/pDNA compared to the mice treated with naked pDNA (5.5-fold) or PEI/pDNA (3.0-fold). This might be due to the superior serum stability of the lamellar phase and high fusion property with the endosome membrane in **RLS5**, resulting in the same satisfying transfection efficiency *in vivo*.

Likely, we examined the EGFP expression in nude mice through an intramuscular injection of **RLS5**/mEGFP as the same administration method as the mRNA vaccine. In the mice injected with naked mRNA, fluorescence was kept for 2 days post-administration at the intramuscular injection site (Fig. 8(B)). Notably, with **RLS5**/mRNA administration, the fluorescence gradually increased, peaked on day 5, and decreased on day 7. In the inter-group comparison, the average fluorescence intensity detected in the mice treated with **RLS5**/mRNA was comparable to that of naked mRNA on day 1, while increased up to 10-fold higher on day 5 (Fig. 8(D)). As the detection sensitivity and specificity of mEGFP were much lower than luciferase,[46] there was a strong background signal existed in the study of mRNA transfection effect *in vivo*. To avoid interference, we only calculated the average fluorescence intensity in the blue circle for the quantitative analysis.

Overall, direct injection of pDNA/mRNA could lead to transgene expression, but the level was significantly low, which was generally considered insufficient to achieve a therapeutic effect.[47] The presence of gene carriers of **RLS5** was necessary to achieve efficient transgene expression *in vivo* for both pDNA and mRNA.

Conclusions

Our previous studies on the structure–activity relationship have pointed out the advantages of second-generation arginine as the hydrophilic part and disulfide bond as the linker in gene delivery systems. In this research, we further designed a series of single-component self-assembled cationic lipids (**RLS1–6**), studied the structure–activity relationship of the hydrophobic part, and explored the potential molecular mechanism affecting the various performance of gene carriers. The cationic lipids contain hydrophobic parts composed of alkyl chains with different lengths, unsaturation, and numbers. Research showed that the introduction of unsaturation could greatly improve the transfection effect, even significantly better than lipofectamine 2000. Mechanism exploration confirmed that the unsaturated bonds could dramatically improve the membrane fluidity and fusion of lipid nanoparticles, increasing the interaction with biological membranes to promote endocytosis and endosomal escape. During the screening, we found that the unsaturation of the alkyl chain had the greatest influence on the performance of lipid nanoparticles, followed by the number of hydrophobic tails. After screening, the optimized **RLS5** with the lamellar phase was the best-performing cationic lipid, with a superior transfection efficiency of pDNA and mRNA *in vivo*, which has potential clinical translational value in the disease prevention and treatment. There are still some shortcomings in this study; for example, (1) more control materials need to be designed to further investigate the influence of alkyl chain unsaturation and quantity, (2) the *in vivo* behavior of lipid nanoparticles needs to be further investigated, such as tissue distribution, metabolic pathway, and long-term toxicity, *etc.* Nevertheless, this study provides reference and important guidance for the design and optimization of lipid gene carriers based on molecular characterization of lipid and cell membrane interactions. Our future studies will contribute to the further development of lipid pDNA and mRNA delivery systems.

Author contributions

Yu Wei and Ting He: conceptualization, methodology, investigation, writing – original draft. Qunjie Bi, Huan Yang, and Xueyi Hu: part of cell and animal experiments. Yongqun Zhu and Rongsheng Tong: validation. Rongrong Jin: visualization, funding acquisition. Hong Liang and Yu Nie: writing – review & editing, supervision, funding acquisition.

Conflicts of interest

There are no conflicts to declare.

Acknowledgements

This work was financially supported by National Natural Science Foundation of China (NSFC, No. 81873921 and 51903174), Sino-German Cooperation Group Project (GZ1512), Chengdu Science and Technology Program (2020-GH02-00007-HZ), Sichuan Science and Technology Program (23GJHZ0001), Miaozi Project in Science and Technology Innovation Program of Sichuan Province (2021024). Postdoctoral Science Foundation of Sichuan

Province (TB2022047). Postdoctoral Science Foundation of Sichuan Academy of Medical Sciences & Sichuan Provincial People's Hospital (2022BH04). Open project foundation of Personalized Drug Therapy Key Laboratory of Sichuan Province (2022YB02). We acknowledged the Analytical & Testing Center, Sichuan University for sample analysis. In addition, we acknowledged Prof. Mattias Barz and Heyang Zhang (Leiden Academic Center for Drug Research, Leiden University) for their help in reviewing & editing.

Notes and references

1 D. Pushparajah, S. Jimenez, S. Wong, H. Alattas, N. Nafissi and R. A. Slavcev, *Adv. Drug Delivery Rev.*, 2021, **170**, 113–141.
2 Y. Klapper, O. A. Hamad, Y. Teramura, G. Leneweit, G. U. Nienhaus, D. Ricklin, J. D. Lambris, K. N. Ekdahl and B. Nilsson, *Biomaterials*, 2014, **35**, 3688–3696.
3 E. S. Fried, J. Luchan and M. L. Gilchrist, *Langmuir*, 2016, **32**, 3470–3475.
4 A. R. Nanna, A. V. Kel'in, C. Theile, J. M. Pierson, Z. X. Voo, A. Garg, J. K. Nair, M. A. Maier, K. Fitzgerald and C. Rader, *Nucleic Acids Res.*, 2020, **48**, 5281–5293.
5 A. Norman, C. Franck, M. Christie, P. M. E. Hawkins, K. Patel, A. S. Ashhurst, A. Aggarwal, J. K. K. Low, R. Siddiquee, C. L. Ashley, M. Steain, J. A. Triccas, S. Turville, J. P. Mackay, T. Passioura and R. J. Payne, *ACS Cent. Sci.*, 2021, **7**, 1001–1008.
6 M. Li, S. Li, Y. Huang, H. Chen, S. Zhang, Z. Zhang, W. Wu, X. Zeng, B. Zhou and B. Li, *Adv. Mater.*, 2021, **33**, e2101707.
7 S. T. LoPresti, M. L. Arral, N. Chaudhary and K. A. Whitehead, *J. Controlled Release*, 2022, **345**, 819–831.
8 Y. Zhang, T. Chu, L. Sun, X. Chen, W. Zhang, H. Zhang, B. Han, J. Chang, Y. Feng and F. Song, *J. Biomed. Mater. Res., Part A*, 2020, **108**, 2409–2420.
9 H. Liang, A. Hu, X. Chen, R. Jin, K. Wang, B. Ke and Y. Nie, *J. Mater. Chem. B*, 2019, **7**, 915–926.
10 X. Yan, L. Lin, S. Li, W. Wang, B. Chen, S. Jiang, S. Liu, X. Ma and X. Yu, *Chem. Eng. J.*, 2020, **395**, 125171.
11 M. Hao, L. Zhang and P. Chen, *Int. J. Mol. Sci.*, 2022, **23**, 9038.
12 T. Nakamura, T. Nakade, K. Yamada, Y. Sato and H. Harashima, *Int. J. Pharm.*, 2021, **609**, 121140.
13 J. Shi, S. Yu, J. Zhu, D. Zhi, Y. Zhao, S. Cui and S. Zhang, *Colloids Surf., B*, 2016, **141**, 417–422.
14 Y. Wu, L. Li, Q. Chen, Y. Su, P. A. Levkin and G. Davidson, *ACS Comb. Sci.*, 2016, **18**, 43–50.
15 S. Liu, Q. Cheng, T. Wei, X. Yu, L. T. Johnson, L. Farbiak and D. J. Siegwart, *Nat. Mater.*, 2021, **20**, 701–710.
16 V. A. Duong, T. T. L. Nguyen and H. J. Maeng, *Molecules*, 2020, **25**, 4781.
17 H. Zhang, J. Leal, M. R. Soto, H. D. C. Smyth and D. Ghosh, *Pharmaceutics*, 2020, **12**, 1042.
18 S. He, W. Fan, N. Wu, J. Zhu, Y. Miao, X. Miao, F. Li, X. Zhang and Y. Gan, *Nano Lett.*, 2018, **18**, 2411–2419.
19 F. G. Wu, H. Y. Sun, Y. Zhou, R. G. Wu and Z. W. Yu, *RSC Adv.*, 2014, **4**, 51171–51179.
20 X. Chen, J. Yang, H. Liang, Q. Jiang, B. Ke and Y. Nie, *J. Mater. Chem. B*, 2017, **5**, 1482–1497.
21 D. Zhang, E. N. Atochina-Vasserman, D. S. Maurya, M. Liu, Q. Xiao, J. Lu, G. Lauri, N. Ona, E. K. Reagan, H. Ni, D. Weissman and V. Percec, *J. Am. Chem. Soc.*, 2021, **143**, 17975–17982.
22 D. Zhi, S. Zhang, B. Wang, Y. Zhao, B. Yang and S. Yu, *Bioconjugate Chem.*, 2010, **21**, 563–577.
23 I. S. Zuhorn, V. Oberle, W. H. Visser, J. Engberts, U. Bakowsky, E. Polushkin and D. Hoekstra, *Biophys. J.*, 2002, **83**, 2096–2108.
24 H. J. Wang, Y. H. Liu, J. Zhang, Y. Zhang, Y. Xia and X. Q. Yu, *Biomater. Sci.*, 2014, **2**, 1460–1470.
25 J. Qiu, L. Kong, X. Cao, A. Li, P. Wei, L. Wang, S. Mignani, A.-M. Caminade, J. P. Majoral and X. Shi, *Nanomaterials*, 2018, **8**, 131.
26 Z. Huang, Y. M. Zhang, Q. Cheng, J. Zhang, Y. H. Liu, B. Wang and X. Q. Yu, *J. Mater. Chem. B*, 2016, **4**, 5575–5584.
27 K. J. Whittlesey and L. D. Shea, *Biomaterials*, 2006, **27**, 2477–2486.
28 M. O. Aviles, C. H. Lin, M. Zelivyanskaya, J. G. Graham, R. M. Boehler, P. B. Messersmith and L. D. Shea, *Biomaterials*, 2010, **31**, 1140–1147.
29 H. Liang, X. Chen, R. Jin, B. Ke, M. Barz, H. Ai and Y. Nie, *Small*, 2020, **16**, e1906538.
30 Q. Jiang, D. Yue, Y. Nie, X. Xu, Y. He, S. Zhang, E. Wagner and Z. Gu, *Mol. Pharmacol.*, 2016, **13**, 1809–1821.
31 S. F. Gilmore, T. S. Carpenter, H. I. Ingolfsson, S. K. G. Peters, P. T. Henderson, C. D. Blanchette and N. O. Fischer, *Nanoscale*, 2018, **10**, 7420–7430.
32 M. Kanduc, E. Schneck and R. R. Netz, *Langmuir*, 2013, **29**, 9126–9137.
33 S. Son, R. Namgung, J. Kim, K. Singha and W. J. Kim, *Acc. Chem. Res.*, 2012, **45**, 1100–1112.
34 S. Arpicco, S. Canevari, M. Ceruti, E. Galmozzi, F. Rocco and L. Cattel, *Farmaco*, 2004, **59**, 869–878.
35 Y. Inoh, T. Furuno, N. Hirashima, D. Kitamoto and M. Nakanishi, *Int. J. Pharm.*, 2010, **398**, 225–230.
36 O. Paecharoenchai, N. Niyomtham, L. Leksantikul, T. Ngawhirunpat, T. Rojanarata, B. E. Yingyongnarongkul and P. Opanasopit, *AAPS PharmSciTech*, 2014, **15**, 722–730.
37 C. H. Jones, C. K. Chen, A. Ravikrishnan, S. Rane and B. A. Pfeifer, *Mol. Pharmaceutics*, 2013, **10**, 4082–4098.
38 H. Zhou, J. Yang, Y. Du, S. Fu, C. Song, D. Zhi, Y. Zhao, H. Chen, S. Zhang and S. Zhang, *Bioorg. Med. Chem.*, 2018, **26**, 3535–3540.
39 G. V. Srilakshmi, J. Sen, A. Chaudhuri, Y. Ramadas and N. M. Rao, *Biochim. Biophys. Acta, Biomembr.*, 2002, **1559**, 87–95.
40 N. Means, C. K. Elechalawar, W. R. Chen, R. Bhattacharya and P. Mukherjee, *Mol. Aspects Med.*, 2022, **83**, 100993.
41 J. Zhang, S. Shrivastava, R. O. Cleveland and T. H. Rabbitts, *ACS Appl. Mater. Interfaces*, 2019, **11**, 10481–10491.
42 Y. Tokudome, Y. Saito, F. Sato, M. Kikuchi, T. Hinokitani and K. Goto, *Colloids Surf., B*, 2009, **73**, 92–96.
43 K. Hayashi, T. Shimanouchi, K. Kato, T. Miyazaki, A. Nakamura and H. Umakoshi, *Colloids Surf., B*, 2011, **87**, 28–35.

44 A. Bouraoui, M. Berchel, R. Ghanem, V. Vie, G. Paboeuf, L. Deschamps, O. Lozach, T. Le Gall, T. Montier and P. A. Jaffres, *Org. Biomol. Chem.*, 2019, **17**, 3609–3616.
45 T. Colombani, P. Peuziat, L. Dallet, T. Haudebourg, M. Mevel, M. Berchel, O. Lambert, D. Habrant and B. Pitard, *J. Controlled Release*, 2017, **249**, 131–142.
46 T. Taheri, H. Saberi Nik, N. Seyed, F. Doustdari, M. H. Etemadzadeh, F. Torkashvand and S. Rafati, *Exp. Parasitol.*, 2015, **150**, 44–55.
47 L. M. Molle, C. H. Smyth, D. Yuen and A. P. R. Johnston, *Wiley Interdiscip. Rev.: Nanomed. Nanobiotechnol.*, 2022, **14**, e1809.